

Design and Characteristics Investigation of Novel Dual Stator Pseudo-Pole Five-Phase Permanent Magnet Synchronous Generator for Wind Power Application

RAJA RAM KUMAR¹, PRIYANKA DEVI¹, CHANDAN CHETRI¹,
AANCHAL SINGH S. VARDHAN², RAJVIKRAM MADURAI ELAVARASAN³,
LUCIAN MIHET-POPA⁴, (Senior Member, IEEE), AND R. K. SAKET⁵, (Senior Member, IEEE)

¹Department of Electrical Engineering, Jorhat Engineering College, Jorhat 785007, India

²Department of Electrical Engineering, Shri G.S. Institute of Technology and Science, Indore 452003, India

³Electrical and Automotive Parts Manufacturing Unit, AA Industries, Chennai 600123, India

⁴Faculty of Engineering, Østfold University College, 1757 Halden, Norway

⁵Department of Electrical Engineering, India Institute of Technology (BHU) Varanasi, Varanasi 221005, India

Corresponding authors: Rajvikram Madurai Elavarasan (rajvikram787@gmail.com) and Lucian Mihet-Popa (lucian.mihet@hiof.no)

ABSTRACT The main focus of this paper is to design and assess the characteristics investigation of Novel Dual Stator Pseudo-Pole Five Phase Permanent Magnet Synchronous Generator (NDSPPFP-PMSG) for wind power application. The proposed generator has a dual stator and two sets of five phase windings which enhance its power density and fault tolerant capability. The novelty of this generator is based on the fact that, eight magnetic poles are formed using only four poles of actual magnets on both the surfaces of the rotor. For the designing and optimal electromagnetic performance of the proposed generator, a Dynamic Magnetic Circuit Model (DMCM) is reported. To validate the results obtained from DMCM, Finite Element Method (FEM) has been opted owing to its high accuracy. For showing the performance superiority, the proposed generator is compared with two conventional generators namely, Dual Stator Embedded-Pole Five Phase (DSEFP) and Single Stator Single Rotor Five Phase (SSSRFP) PMSG. To compare their performances, FEM results are considered. The electromagnetic performance namely, generated Electromotive Force (EMF), percentage (%) Total Harmonic Distortion (THD) of generated EMF, generated EMF vs speed, terminal voltage vs load current, electromagnetic torque developed on rotor vs time, %ripple content in the torque, and %efficiency vs load current are investigated for all the three generators. From these investigations, it is found that the power density (power to weight ratio) of the proposed generator is maximum.

INDEX TERMS Dual stator, dynamic magnetic circuit model, embedded-pole, finite element method, five phase, permanent magnet synchronous generator, pseudo pole, single stator single rotor, wind power.

I. INTRODUCTION

In order to meet the growing load demands, along with the use of fossil fuels, non-conventional sources of energy are also relied on. These energies are sustainable in nature, reduces the risk of harmful emissions from greenhouse gases and undoubtedly benefits the people for a longer-term future [1]. The major non-conventional sources of energy are solar, wind, geothermal, biomass, hydro, etc. Amongst these,

The associate editor coordinating the review of this manuscript and approving it for publication was Weixing Li.

wind energy is the cleanest and fastest-growing energy source [2], [3]. It has numerous benefits, such as it is cheaper, eco-friendly emission free and can provide an excellent alternative to the fossil fuels [4]–[6].

For the generation of huge power from wind energy, large wind farms are required which consists of several wind turbine systems connected to the electrical grid. These wind farms can be located either in the onshore (in-land) or offshore (in-water bodies) [7], [8]. The installation of offshore turbines is very costly unlike onshore, as they are fixed in water bodies like the sea, ocean, etc., hence, they require a

strong supporting structure [9]. Also, special types of cables and equipment are needed in the system which can withstand the salinity of water.

Hence, it can be concluded that for the transmission of electrical energy, the onshore turbines are significantly cheaper than that of the offshore ones. From the past decades, the on-shore wind turbines have been utilized for power generation, due to which the technologies used in onshore are well developed compared to the offshore [10], [11]. A schematic diagram of the general wind power system with the components such as, wind-turbine, synchronous generator, rectifier, inverter, transformer and grid is shown in Fig. 1.

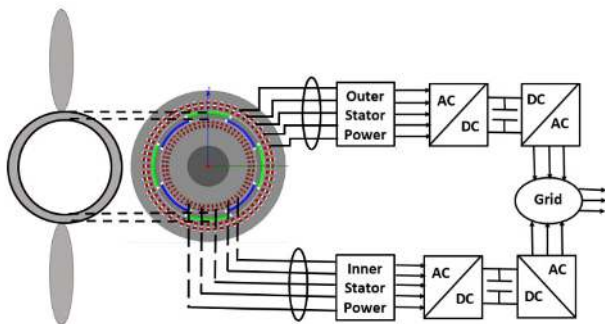


FIGURE 1. Model of wind-power system.

Considerable research has been done in the field of wind-power generation in order to design a highly suitable generator with special features, so that the power produced from the wind farms can meet the energy demands and supply in an efficient manner [12]–[15]. Several generators are developed and investigated, such as induction and synchronous generator [16]–[18]. Amongst these, the most popular one is the Permanent Magnet Synchronous Generator (PMSG) for the wind turbine [19]. These generators are ideally suited for wind power application as it does not require any gearbox, unlike the induction generators. The gearbox requires regular replacement of oil, creates mechanical vibration and as a result decreases the overall stability of the system. Hence, avoiding gearbox reduces the maintenance cost of the machines [20]–[22]. The PMSG also do not require any slip-rings, rotor windings and external excitation in the rotor [23], [24]. In addition, the PMSG has several advantages such as it provides high-power density and efficiency, absence of additional noise in the system, light weight, etc. [25]–[27].

Several topologies for PMSG have been investigated in many literatures, such as single stator and dual stator systems [28]. The single stator system is the simplest one which is used in conventional generators. The dual stator system provides high power generation in comparison to a single stator [29]. There are total two air gaps in this dual stator system, which results in the addition of the Magnetomotive Force (MMF) created by the inner and outer sets of magnets in the rotor. Hence, this system generates more EMF in comparison to a single stator system [30]. To further improve the torque density, the multiphase system (more than 3-phase)

can be considered. The Multiphase system offers a higher degree of freedom under-faulted conditions, i.e. it can operate continuously even if one or two phases are faulty [31], [32].

From various studies, it has been observed that the orientation of magnets in the rotor is also an important aspect to enhance the total flux linkage as well as the power density of the generator. Based on this factor, the PMSGs are primarily classified into embedded-pole or surface-mounted [33], [34]. In the surface-mounted configuration, the arc-shaped magnets are attached on the surface of rotor [35]. This orientation helps in reducing the leakage flux in the generator to a major extent. In [36], the magnets are attached to the rotor surface with the help of permanent magnet sleeve which are either made up of metallic or non-metallic materials. These sleeves firmly hold the magnets, thus can be used for high speed applications [37], [38]. But the presence of these sleeves increases the air gap between magnets and the windings, thus, reduces the overall air-gap flux density of the generator [39]. In [40], the magnets are attached to the rotor without using sleeves with the help of adhesives. This orientation of the magnets will increase the overall airgap flux density of the generator. In embedded pole system [41], the permanent magnets are buried in the rotor firmly which makes the model complex. The embedded-pole magnets are more reliable and robust as compared to surface-mounted PMSG [42]–[45]. Nevertheless, the close proximity of magnets to both the inner and outer stator windings often lead to demagnetization of the magnets due to persistent heat from the windings which effects the overall functionality of PMSG [46]. In [47], a new orientation of magnet has been reported i.e. pseudo-pole magnets for improving the power density of the generator. In this model, a particular portion of the ferromagnetic rotor is itself considered as pseudo-pole.

Keeping this point in mind, the authors have used the concept of pseudo-pole to design and perform characteristic investigation of Novel model for Wind-Power Application i.e. Novel Dual Stator Pseudo-Pole Five-Phase (NDSPPFP) Permanent Magnet Synchronous Generator (PMSG). A five-phase system is used as the ripple and cogging torque are very less in it, compared to the 3-phase system [48], [49]. The main objective of using the pseudo-pole is to produce high and uniform flux from the permanent magnets. In pseudo-pole generator, unlike conventional generator, the requirement of total magnetic poles is less. In fact, in comparison to the embedded pole, it was observed that the Pseudo pole generator model is not that complex, provided that both have the same volume of magnets. For designing and performance evaluation of generators, two types of analysis are very popular namely, analytical and numerical. Analytical method of analysis is very simple and fast to optimize and evaluate the performance of generator [50]. Analytical methods are of many types namely, Reluctance Network Method (RNM), sub domain modeling technique method, Fourier analysis method, Fourier transform method, etc. Out of these analytical techniques RNM is the simplest and accurate method for the performance analysis of generator. In RNM, a dynamic

modeling is done where a magnetic network for the optimal designing is formed [51]. This magnetic network predicts the performance of the generator. Here for evaluation, few parameters are considered to get accuracy in results such as, reluctance of the different portion, leakage flux, material properties, saturation effect and MMF sources. In [52], the parameter such as leakage-flux, saturation effect and core material are considered and in [53], flux-leakage parameter is taken. Similarly, in [54], the saturation effect and core material are evaluated. From these studies, it was observed that the combined effect of all the parameters (reluctances, leakage flux, material properties, saturation effect and MMF sources) was not yet discussed. Taking all the parameters together while modeling is important because if number of parameters considered are high, then undoubtedly, the predicted value of machine performance will be more exact.

Thus, the authors proposed Dynamic Magnetic Circuit Model (DMCM) for the NDSPPFP-PMSG by considering all the above-discussed parameters. Using this circuit, we can predict the performance in shorter time. To validate the predicted results of analytical method, the numerical analysis is done. Finite Element Method (FEM) in the numerical analysis is popular, as it gives most accurate results. Though it is time consuming [55] but still this method is used widely for validating the results precisely, which is obtained from DMCM. Therefore, both DMCM and FEM analysis of the proposed model is done for the evaluation purpose in order to obtain accurate results.

As per authors' information, the pseudo-pole magnet system is introduced for the first time in dual stator five-phase system, and hence, can be considered as novel. To prove its superiority, this model is compared with the dual stator embedded-pole PMSG and single stator conventional generators. The winding arrangement on both the inner and the outer stator is of five-phase and also the iron volume, winding, and magnetic span are kept same for all the three models.

The following points highlights the objectives of this paper:

- A Novel Dual Stator Pseudo-Pole PMSG has been proposed for wind power application.
- A Dynamic Magnetic Circuit Modeling (DMCM) has also been proposed for the NDSPPFP-PMSG and for validation of the results, FEM has been opted as it gives accurate results.
- To prove the superiority of the proposed NDSPPFP-PMSG, a comparison is made with two conventional generators namely, DSEPFP-PMSG and SSSRFP-PMSG. For this purpose, the results of FEM analysis are considered owing to its high accuracy.

The paper has been divided in the following manner: Section II introduces the generator topologies, stator and rotor structure description and their operating principle for all the three models. The FEM and Analytical analysis for each model is included in the Section III and results are reported in Section IV. Finally, in Section V, the concluding remarks has been presented.

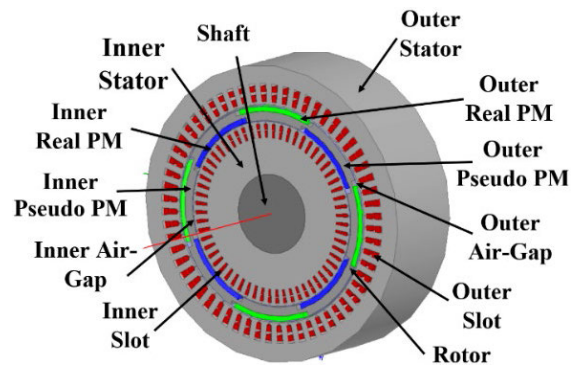


FIGURE 2. Schematic diagram of NDSPPFP-PMSG.

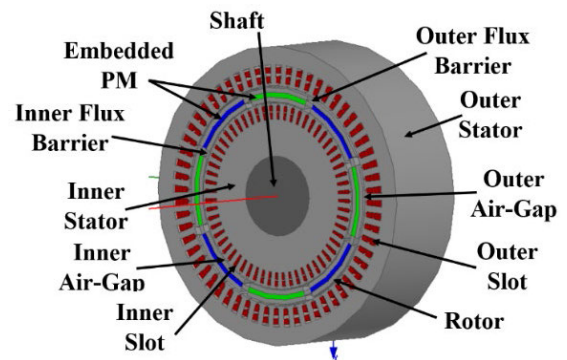


FIGURE 3. Schematic diagram of DSEPFP-PMSG.

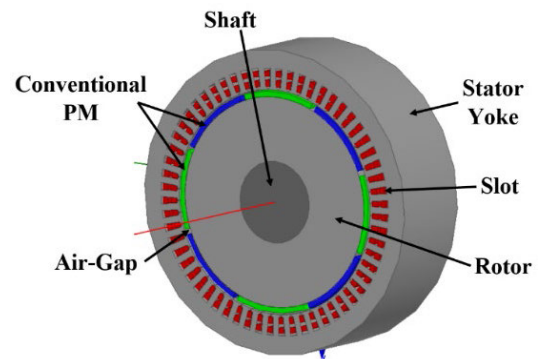


FIGURE 4. Schematic diagram of SSSRFP-PMSG.

II. GENERATOR TOPOLOGIES AND OPERATING PRINCIPLE

A. GENERATOR TOPOLOGIES

The structure of the proposed Novel Dual Stator Pseudo Pole Five Phase (NDSPPFP), Dual Stator Embedded Pole Five Phase (DSEPFP) and Single Stator Single Rotor Five-Phase (SSSRFP) PMSG are shown in Fig. 2, Fig. 3 and Fig. 4 respectively. The NDSPPFP-PMSG and DSEPFP-PMSG consists of dual stators and single rotor, i.e. inner and outer stator-rotor system. The SSSRFP-PMSG has only one stator-rotor system whose dimensions are similar to the outer stator rotor system of NDSPPFP-PMSG and DSEPFP-PMSG. The details of design parameters for these three generators are enlisted in Table 1. The design parameters of

TABLE 1. Design parameters of the PMSGs.

Parameter	NDSPPFP-PMSG	DSEFPFP-PMSG	SSSRFP-PMSG	Unit
Outer diameter of outer stator	300	300	300	mm
Inner diameter of outer stator	220	220	220	mm
Height of magnet	5	5	5	mm
Air-Gap Length	1.5	1.5	1.5	mm
Thickness of rotor yoke	4	14	63.5	mm
Outer diameter of inner stator	186	186	-	mm
Inner diameter of inner stator	80	80	-	mm
Diameter of shaft	80	80	80	mm
No. of outer stator slots	60	60	60	mm
No. of inner stator slots	60	60	-	mm
No. of poles	8	8	8	-

all the three generators are kept almost similar for accurate results.

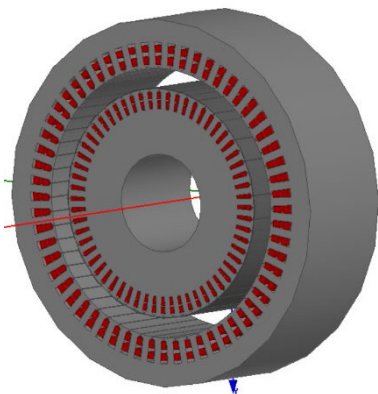


FIGURE 5. Stators of NDSPPFP-PMSG and DSEFPFP-PMSG.

1) STATOR DESCRIPTION

The NDSPPFP-PMSG and DSEFPFP-PMSG consist of two stators namely, outer and inner stator. Both these stators have 60 slots comprising of 8-poles fractional slot five-phase balanced distributed windings as shown in Fig. 5. These five phases are separated by 72° electrical from each other and each phase winding consists of 12 coils. The inner stator winding coils have 15 turns whereas the outer stator winding coils have 30 turns. Similarly, SSSRFP-PMSG has single stator which has 60 slots comprising of 8-poles fractional slot five-phase balanced distributed winding as shown in Fig. 6.

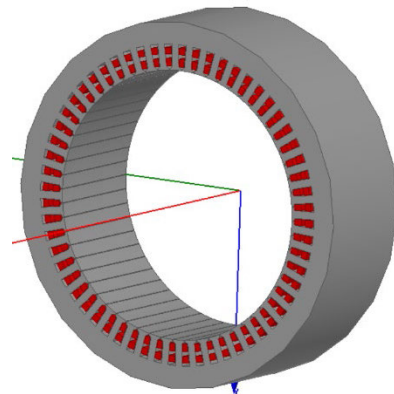


FIGURE 6. Schematic diagram of SSSRFP-PMSG.

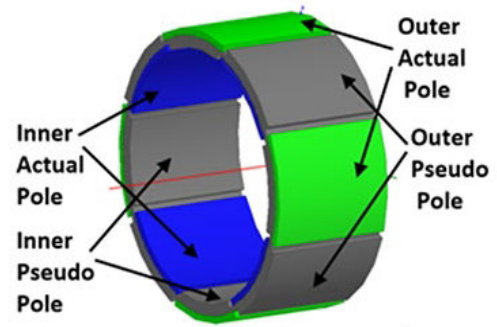


FIGURE 7. Schematic diagram of the rotor of NDSPPFP-PMSG.

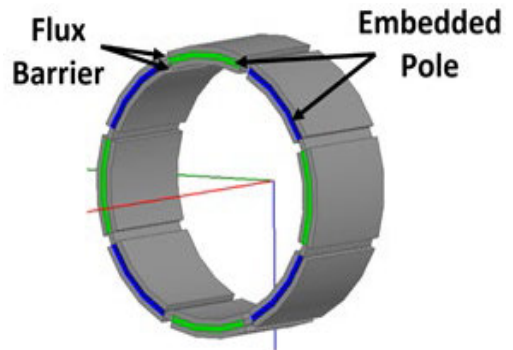


FIGURE 8. Schematic diagram of the rotor of DSEFPFP-PMSG.

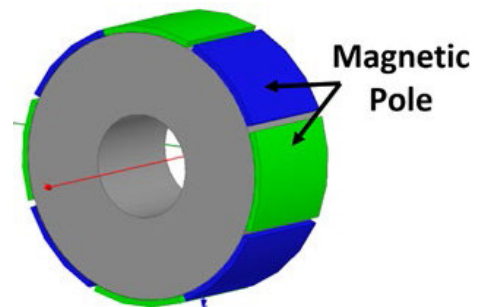
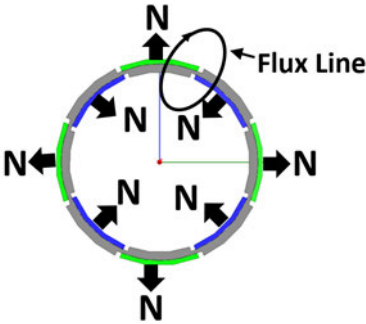
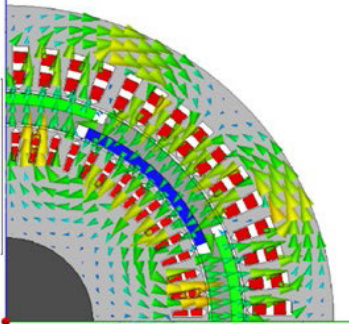
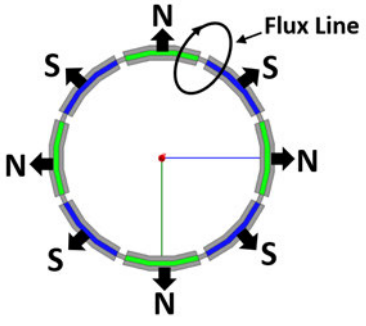
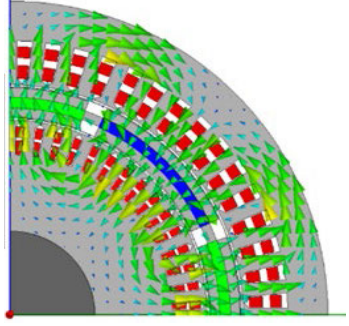
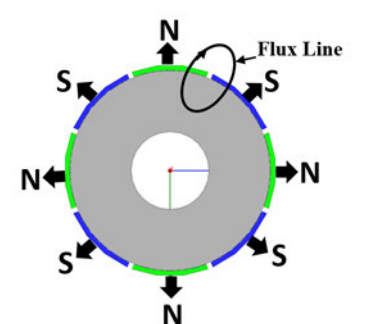
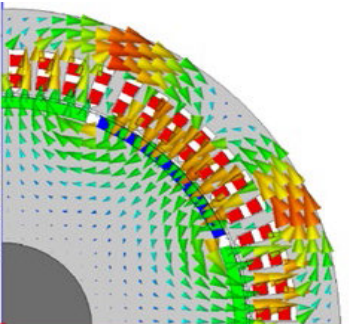


FIGURE 9. Schematic diagram of the rotor of SSSRFP-PMSG.

2) ROTOR AND MAGNETIC POLE CONFIGURATION

The NDSPPFP, DSEFPFP and SSSRFP-PMSG have a single rotor of different structure as shown in Fig. 7, Fig. 8 and Fig. 9 respectively. The rotor of proposed generator has

TABLE 2. Principle of operation of the PMSGs.

Model	Representation of flux lines	Flow of flux lines
NDSPPFP-PMSG		
DSEFPFP-PMSG		
SSSRFP-PMSG		

4-actual poles with an arc span of 45° mounted on both the surfaces of rotor. Whereas a total of 4-pseudo poles are formed in the extended portions on the surface of the rotor iron yoke in the proposed generator. Similarly, the rotor of DSEFPFP generator has 8-actual poles embedded poles in the rotor. The flux barriers are provided in between the two magnets in upper and lower portion of rotor so that the flux does not get linked with each other. On the other hand, conventional SSSRFP has 8-poles mounted on the rotor surface. The air-gap length of all the three generators are kept same. The magnets in the rotor are firmly attached using adhesive elements. The green and blue colour depict north and south magnets in the rotor.

B. PRINCIPLE OF OPERATION

Table 2 shows the operating principle of all the three generators. There are total three columns in the table, the first column represents the name of different models, the second and third column depicts the rotors with their flux line formation and vector plot of flux lines flow respectively in one quarter of model. The rotor of the proposed NDSPPFP-PMSG comprises of a rotor yoke and two actual magnets which act as north-pole for the formation of two poles. The extended portion of the rotor on both the inner and outer surfaces receives all the flux incident on the surface and acts like a pseudo south-pole, thus avoids the leakage of fluxes from this portion. The vector plot of the proposed model in Table 2

shows the flow of fluxes resulting due to the placement of the magnets on the rotor. The DSEFPF-PMSG has magnetic poles which are embedded inside the rotor. In order to ensure that the magnets are in equal distance from both the airgaps, the magnetic poles are embedded in the middle of the rotor yoke. The flux barriers are provided in between the magnetic poles on both the surfaces of the rotor in order to avoid magnetic flux leakage and hence improves the power density of the generator. The path of flow of the flux lines is represented by the vector plot of flux lines in the quarter part of the model. Similarly, the flow of flux and magnetic poles on the surface of the rotor for the conventional SSSRFP-PMSG is shown in the table 2.

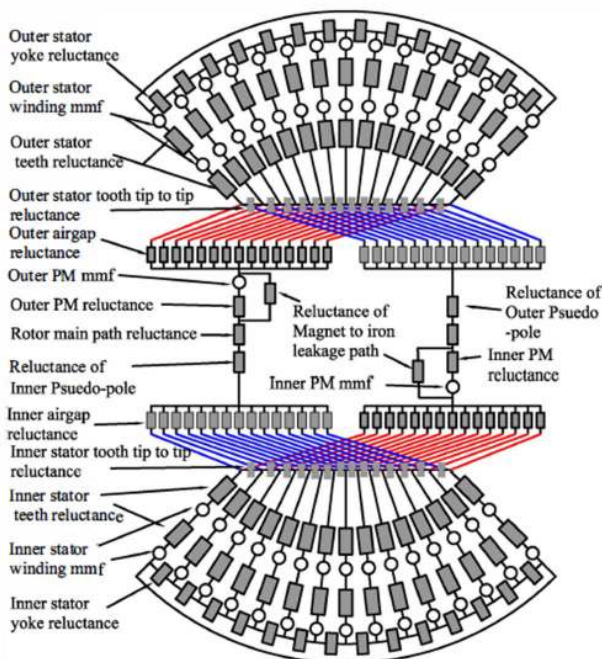


FIGURE 10. DMCM of NDSPPFP-PMSG.

III. DYNAMIC MAGNETIC CIRCUIT MODELING

The dynamic magnetic circuit modeling used for accurate design and performance optimization of the proposed NDSPPFP generator. Fig. 10 presents a DMCM for the proposed generator. This magnetic circuit network comprises linear, non-linear and dynamic reluctances with MMF sources. The linear reluctances in the model are namely, stator tooth tip to tip, actual magnetic poles and magnet to rotor flux leakage path reluctances for both inner and outer portion in model. Whereas the Non-linear reluctances are namely, stator (inner and outer) and rotor core reluctances generate due to saturation effect of the core material. Saturation lead to decrease the permeability ought to which increases the reluctance of the core materials that degrades the performance of the generator. The dynamic reluctance in the network are the airgap (inner and outer) reluctances. These vary with the rotor rotation and interaction between actual magnetic pole with stator teeth, as presented in the DMCM. The two

sets of the five-phase winding (inner and outer) and actual magnetic poles are the MMF sources in the network. The winding fluxes depends upon the phase currents (inner and outer) whereas the flux due to permanent magnet depends on the properties of magnetic material and the dimensional parameters of the actual poles.

The reluctance network represented in DMCM shows one quarter of the model because of its model symmetry. It consists of 66 nodes, 152 branches and 87 loops at the initial position. Moreover, for its simplicity, the reluctances of outer and inner stator teeth in the branches and winding in the slots can be lumped with its equivalent reluctances and equivalent MMF sources in the stator teeth branches.

The linear and non-linear reluctances of different parts of model are calculated using (1) and (2). There are 15 slots in both the inner and outer portion of stator, each having double layered winding. The MMF sources due to these winding are represented with the stator teeth in its upper and lower portion. The magnitude of these sources can be computed with phase currents using (3).

The dynamic airgap reluctances depend upon the rotor position and the interaction between actual Permanent Magnet (PM) and stator teeth. There are total of 15 possible interactions between the first PM and 15 stator teeth.

The reluctances of these portions can be calculated using (4). The reluctances of permanent magnet to rotor leakage path can be calculated using (5). The permanent magnet are the main MMF sources in the network and their magnitude can be calculate using (6). The flux in each part can be calculated using (7) and the reluctances of the network are presented in the (8).

The reluctance of various parts is calculated using below-mentioned relations:

1. Linear Reluctance:

The linear reluctance ($R_{l(i,o)}$) is calculated as:

$$R_{l(i,o)} = \frac{l_{l(i,o)}}{\mu_0 \mu_r A_{l(i,o)}} \quad (1)$$

where $l_{l(i,o)}$ is the length and $A_{l(i,o)}$ is the cross-sectional area of the flux flow of the inner and outer section of the model, μ_0 is the permeability of free space, μ_r is the relative permeability of the material. In the above equation, ‘i’ denotes the inner and ‘o’ denotes the outer.

2. Non-Linear Reluctance:

Similarly, $R_{nl(i,o)}$ is the non-linear reluctance and can be calculated as:

$$R_{nl(i,o)} = \frac{l_{nl(i,o)}}{\mu_0 \mu_{feBnl} A_{nl(i,o)}} \quad (2)$$

where $l_{nl(i,o)}$ is the length and $A_{nl(i,o)}$ is the cross-sectional area of the flux flow of the inner and outer section of the model, μ_{feBnl} is the permeability function which depends upon the flux density in the material.

3. MMF sources:

In Fig. 10, total 15 stator slots are represented having an upper and lower layer of winding in the model. This winding

shows mmf sources which are present in the model with tooth reluctance. These MMF sources are computed with the phase currents as:

$$\begin{aligned} \text{MMF}_{w(i,o)} &= [f_{1(i,o)} f_{2(i,o)} f_{3(i,o)} \dots f_{15(i,o)}]^T \\ &= N_{c(i,o)} \cdot \begin{pmatrix} 2 & 0 & 0 & 0 & 0 \\ 0 & 0 & 0 & -2 & 0 \\ 0 & 1 & 0 & -1 & 0 \\ 0 & 2 & 0 & 0 & 0 \\ 0 & 0 & 0 & 0 & -2 \\ 0 & 0 & 1 & 0 & -1 \\ 0 & 0 & 2 & 0 & 0 \\ -2 & 0 & 0 & 0 & 0 \\ -1 & 0 & 0 & 1 & 0 \\ 0 & 0 & 0 & 2 & 0 \\ 0 & -2 & 0 & 0 & 0 \\ 0 & -1 & 0 & 0 & 1 \\ 0 & 0 & 0 & 0 & 2 \\ 0 & 0 & -2 & 0 & 0 \\ 1 & 0 & -1 & 0 & 0 \end{pmatrix} \cdot \begin{pmatrix} I_{a(i,o)} \\ I_{b(i,o)} \\ I_{c(i,o)} \\ I_{d(i,o)} \\ I_{e(i,o)} \end{pmatrix} \end{aligned} \quad (3)$$

where $f_{1(i,o)}, f_{2(i,o)}, f_{3(i,o)}, \dots, f_{15(i,o)}$ are the sources of MMF linked to the corresponding stator tooth branches of inner and outer section, T denotes the transpose of the matrix and $N_{c(i,o)}$ is the number of turns per phase in the inner and outer stator winding.

4. Reluctance of Air-Gap:

The calculation of the air gap reluctance is not that simple as the rotor keeps on rotating during operating condition. It is based on the interaction of PMs and stator tooth. In Fig. 10, there are 15 reluctances with one PM interaction in the reluctance network and these reluctances can be computed using:

$$R_{gi(i,o)} = \frac{g_{(i,o)}}{\mu_0 \cdot \text{width}_{(i,o)} \cdot L} \quad (4)$$

where, $\text{width}_{(i,o)} = r_{g(i,o)} \cdot \theta_{t-pm(i,o)}$ and $\theta_{t-pm(i,o)}$ is the interaction angle between tooth of the inner and outer section and PM. $r_{g(i,o)}$ is the radius of the inner and outer airgap and $g_{(i,o)}$ is the length of outer and inner airgap.

5. Reluctance of the magnet to rotor iron leakage flux path:

Reluctance of magnet to rotor iron leakage flux path for the inner and outer section ($R_{mi(i,o)}$) [56]

$$R_{mi(i,o)} = \frac{\pi}{\mu_0 L \ln \left(1 + \frac{\pi g_{eff(i,o)}}{H_{pm}} \right)} \quad (5)$$

where, $g_{eff(i,o)}$ is the effective airgap length of the inner and outer airgap. H_{pm} is the height of the magnet (both are equal), L is the core length of the generator.

6. MMF due to actual and pseudo-magnet:

The magnets in the rotor are the main MMF sources in this network and can be computed as:

$$\text{MMF}_{pm(i,o)} = H_c \cdot H_{pm} \quad (6)$$

where H_c is the coercivity and H_{pm} is the height of PM (equal height of the inner and outer PM) in the direction of magnetization.

The Reluctance Network Method (RNM) results in a set of linear equations which should be solved to obtain the magnetic fluxes of the inner and outer section.

$$[\phi] = [R]^{-1} [\text{MMF}_{(i,o)}] \quad (7)$$

$$[R] = \begin{pmatrix} R_{1,1} & \dots & R_{1,87} \\ \vdots & \ddots & \vdots \\ R_{87,1} & \dots & R_{87,87} \end{pmatrix} \quad (8)$$

where R is (87×87), MMF is (87×1) and the flux (Φ) is (87×1) matrix corresponding to model.

A. FIELD DENSITY AND PERFORMANCE INVESTIGATION

Upon observation, it is found that the magnetic flux distribution in the air gap is trapezoidal in shape with slotting effect in which both the halves of the curves are of different magnitude due to the actual and pseudo poles. Due to this unequal shape, all the harmonics are present in the flux density of the inner and outer airgap.

Magnetic flux density due to the PMs (actual and pseudo) in the inner air gap,

$$B_{gi}(\theta_{er}) a_{oi} + \sum_{n=1}^{\infty} (a_{ni} \cos(n\theta_{er}) + b_{ni} \sin n(\theta_{er})) \quad (9)$$

where, θ_{er} is the rotor rotation electrical angle, n is the order of harmonics in the flux density and a_{oi} , a_{ni} and b_{ni} are the

Fourier series constants whose values are

$$a_{oi} = \frac{B_{gi(+ve \max.)}}{2\pi} (1.861\pi - 3.6525\theta_i) \quad (10)$$

$$\begin{aligned} a_{ni} &= \frac{B_{gi(+ve \max.)}}{2\pi n} \left(\frac{\sin n\theta_i}{\theta_i} + 2\cos n\left(\frac{\pi}{2}\right) \cdot \sin n\left(\frac{\pi}{2} - \theta_i\right) \right. \\ &\quad \left. + 1.722 \cos n\left(\frac{3\pi}{2}\right) \cdot \sin n\left(\frac{\pi}{2} - \theta_i\right) + \frac{0.861}{n\theta_i} \right. \\ &\quad \left. - 0.861 \sin n(\theta_i) - \frac{0.861}{n\theta_i} \cos(n\theta_i) \right) \end{aligned} \quad (11)$$

$$\begin{aligned} b_{ni} &= \frac{B_{gi(+ve \max.)}}{2\pi n} \left(\frac{\cos n\theta_i - 1}{\theta_i} - 2\sin n\left(\frac{\pi}{2}\right) \cdot \sin n\left(\frac{\pi}{2} - \theta_i\right) \right. \\ &\quad \left. + \frac{1.861}{\theta_i} \cdot (\pm 1)^n \cdot (\theta_i \cos n(\theta_i) - \frac{\sin n(\theta_i)}{n}) \right. \\ &\quad \left. - 1.722 \sin n\left(\frac{3\pi}{2}\right) \cdot \sin n\left(\frac{\pi}{2} - \theta_i\right) - 0.861 \cos n(\theta_i) \right. \\ &\quad \left. - \frac{0.861}{n\theta_i} \sin(n\theta_i) \right) \end{aligned} \quad (12)$$

$B_{gie}(\theta_{er})$ has two different values of the airgap flux density for the actual and pseudo poles. $B_{gie(+ve \max.)}$ corresponds

to the positive half (actual pole) whereas $B_{gie(-ve\ max.)}$ corresponds to the negative half (pseudo pole). $B_{gie(-ve\ max.)} = 0.861B_{gie(+ve\ max.)}$ and $\theta_i = \frac{\pi}{18}$.

The equivalent airgap flux density in the inner airgap is (B_{gie})

$$B_{gie} = \frac{B_{gi(+ve\ max.)} + B_{gi(-ve\ max.)}}{2} \quad (13)$$

The assumed airgap flux density (trapezoidal in shape) in the inner airgap ($B_{gkiA}(\theta_{er})$)

$$B_{gkiA}(\theta_{er}) = \sum_{k=1,3,5}^{\infty} B_{gkiA} \sin(k\theta_{er}) \quad (14)$$

where

$$B_{gkiA} = \frac{4}{\pi(\frac{\pi}{2} - \beta)} \frac{B_{gie}}{k^2} \cos(k\beta) \sin(k\frac{\pi}{2}) \quad (15)$$

where, k is the order of harmonic present in the assumed inner airgap flux density and β is the angular span of the magnet.

Magnetic flux density due to the PMs in the outer air gap,

$$B_{go}(\theta_{er}) = a_{o0} + \sum_{n=1}^{\infty} (a_{no} \cos(n\theta_{er}) + b_{no} \sin n(\theta_{er})) \quad (16)$$

where, a_{o0} , a_{no} and b_{no} are the Fourier series constants whose values are

$$a_{o0} = \frac{B_{go(+ve\ max.)}}{2\pi} (1.9174\pi - 3.7935\theta_o) \quad (17)$$

$$a_{no} = \frac{B_{go(+ve\ max.)}}{2\pi n} \left(\frac{\sin n\theta_o}{\theta_o} + 2\cos n(\frac{\pi}{2}) \cdot \sin n(\frac{\pi}{2} - \theta_o) + 1.8348 \cos n(\frac{3\pi}{2}) \cdot \sin n(\frac{\pi}{2} - \theta_o) + \frac{0.9174}{n\theta_o} - 0.9174 \sin n(\theta_o) - \frac{0.9174}{n\theta_o} \cos(n\theta_o) \right) \quad (18)$$

$$b_{no} = \frac{B_{go(+ve\ max.)}}{2\pi n} \left(\frac{\cos n\theta_o - 1}{\theta_o} - 2\sin n(\frac{\pi}{2}) \cdot \sin n(\frac{\pi}{2} - \theta_o) + \frac{1.9179}{\theta_o} \cdot (\pm 1)^n \cdot (\theta_o \cos n(\theta_o) - \frac{\sin n(\theta_o)}{n}) - 1.8348 \sin n(\frac{3\pi}{2}) \cdot \sin n(\frac{\pi}{2} - \theta_o) - 0.9174 \cos n(\theta_o) - \frac{0.9174}{n\theta_o} \sin(n\theta_o) \right) \quad (19)$$

$B_{goe}(\theta_{er})$ has two different values of the airgap flux density for the actual and pseudo poles. $B_{goe(+ve\ max.)}$ corresponds to the positive half (actual pole) whereas $B_{goe(-ve\ max.)}$ corresponds to the negative half (pseudo pole). $B_{goe(-ve\ max.)} = 0.9174B_{goe(+ve\ max.)}$ and $\theta_o = \frac{\pi}{18}$.

$$B_{goe} = \frac{B_{go(+ve\ max.)} + B_{go(-ve\ max.)}}{2} \quad (20)$$

The assumed airgap flux density (trapezoidal in shape) in the inner airgap ($B_{gkoA}(\theta_{er})$)

$$B_{gkoA}(\theta_{er}) = \sum_{k=1,3,5}^{\infty} B_{gkoA} \sin(k\theta_{er}) \quad (21)$$

where,

$$B_{gkoA} = \frac{4}{\pi(\frac{\pi}{2} - \beta)} \frac{B_{goe}}{k^2} \cos(k\beta) \sin(k\frac{\pi}{2}) \quad (22)$$

No-load generated EMF of inner and outer stator and average electromagnetic torque required by the generator are represented by (23), (25) and (28) respectively.

Generated voltage in the inner stator winding ($E_i(t)$)

$$E_i(t) = \sum_{k=1,3,7}^{\infty} E_{ki} \sin(kw_e t) \quad (23)$$

where, peak value of inner stator voltage (E_{ki}) is

$$E_{ki} = \frac{16}{P} \times 2.9563 \times N_{ci} L_i r_{si} w_e B_{gkiA} \cos\left(k\frac{\pi}{30}\right) \quad (24)$$

where w_e is the electrical speed of rotor and P is the number of pole, N_{ci} is the total number of conductor per phase in the winding, L_i is the iron length of the core, r_{si} is the radius of inner stator.

Generated voltage in the outer stator winding ($E_o(t)$)

$$E_o(t) = \sum_{k=1,3,7}^{\infty} E_{ko} \sin(kw_e t) \quad (25)$$

where, peak value of outer stator voltage (E_{ko}) is

$$E_{ko} = \frac{16}{P} \times 2.9563 \times N_{co} L_i r_{so} w_e B_{gkoA} \cos\left(k\frac{\pi}{30}\right) \quad (26)$$

and w_e is the electrical speed of rotor and P is the number of pole, N_{ci} is the total number of conductor per phase in the winding, L_i is the iron length of the core, r_{so} is the radius of outer stator.

The total output power (P(t)) is:

$$P(t) = E_{ai}(t) I_{ai}(t) + E_{bi}(t) I_{bi}(t) + E_{ci}(t) I_{ci}(t) + E_{di}(t) I_{di}(t) + E_{ei}(t) I_{ei}(t) + E_{ao}(t) I_{ao}(t) + E_{bo}(t) I_{bo}(t) + E_{co}(t) I_{co}(t) + E_{do}(t) I_{do}(t) + E_{eo}(t) I_{eo}(t) \quad (27)$$

The average electromagnetic torque (T(t)) is

$$T(t) = \frac{P(t)}{w_e} \quad (28)$$

Torque ripple (%)

$$T_{ripple} = \frac{T_{max} - T_{min}}{T_{average}} \times 100\% \quad (29)$$

where, T_{max} is the maximum value of torque and T_{min} is the minimum value of torque and $T_{average}$ is the average torque.

Efficiency (%)

$$\eta = \frac{P_o}{P_o + P_L} \times 100\% \quad (30)$$

where, P_o is the output power and P_L is the loss that includes copper and core loss.

IV. FINITE ELEMENT METHOD

The proposed NDSPPFP-PMSG and DSEFPFP-PMSG both consists of dual stator and single rotor. Here, the outer and inner stator consists of 60 slots, 8-pole, 5-phase windings. The size of the rotor in both these generators are different as described in Table 2. Similarly, SSSRFP-PMSG consists of a single stator and single rotor. The stator consists of 60 slots, 8-pole, 5-phase winding arrangement. The rotor of this conventional generator is described in Table 2.

For the comparison of the electromagnetic performance of all the three generators, Finite Element Method (FEM) has been used as it gives accurate results. Magnetostatic and transient modes of FEM analysis has been used here. The magnetostatic mode of analysis is done to get flux lines and flux density distribution and the transient mode of analysis is done for performance evaluation. For the analysis, some basic steps are followed namely, modeling, assigning material properties and boundaries, providing excitation, meshing, providing analysis set-up, and finally, the results are obtained.

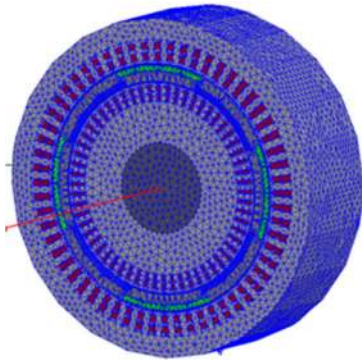


FIGURE 11. Mesh plot of NDSPPFP-PMSG.

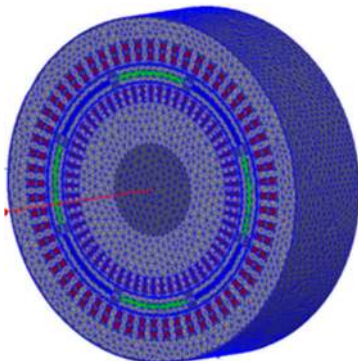


FIGURE 12. Mesh plot of DSEFPFP-PMSG.

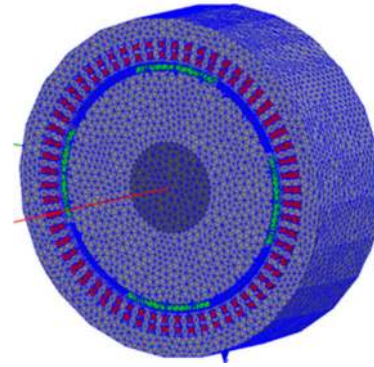


FIGURE 13. Mesh plot of SSSRFP-PMSG.

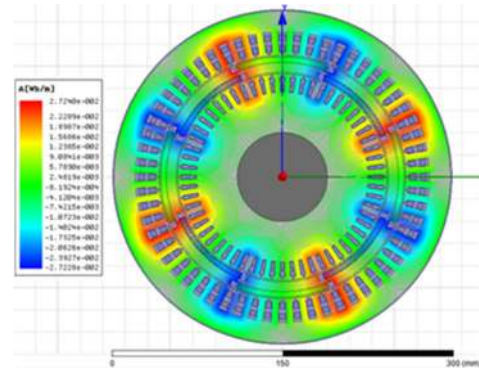


FIGURE 14. Flux line plot of NDSPPFP-PMSG.

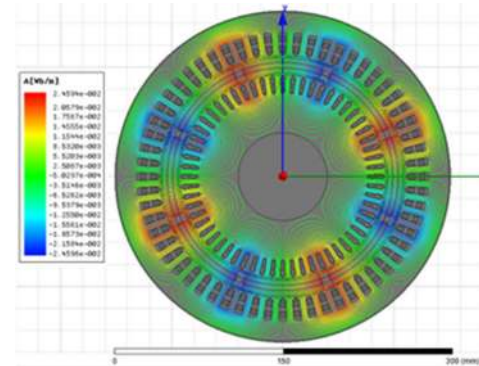


FIGURE 15. Flux line plot of DSEFPFP-PMSG.

Fig. 11, Fig. 12 and Fig. 13 show the mesh plot of NDSPPFP-PMSG, DSEFPFP-PMSG and SSSRFP-PMSG respectively. In meshing, the entire model is divided into small triangular section of different sizes and the analysis in each of these smaller triangular sections is carried out in order to improve the accuracy of the solution obtained. A total number of 429864, 425985 and 370082 mesh elements are formed for the NDSPPFP-PMSG, DSEFPFP-PMSG and SSSRFP-PMSG respectively.

Fig. 14, Fig. 15 and Fig. 16 show the flux line distribution plots for NDSPPFP-PMSG, DSEFPFP-PMSG and SSSRFP-PMSG respectively. In all these three plots, we observe that the 8-contour of flux lines are formed which confirms the formation of 8-poles due to the arrangement of the magnets inside the model.

Fig. 17 shows the flux density distribution in the NDSPPFP generators. It is clear from the plot that the flux density at different portions namely, outer stator yoke, outer stator tooth, rotor yoke, inner stator tooth, and inner stator yoke are 0.944T, 1.13 T, 0.868 T, 1.322 T, 0.944 T respectively. From the above values of flux density, it is observed that the flux

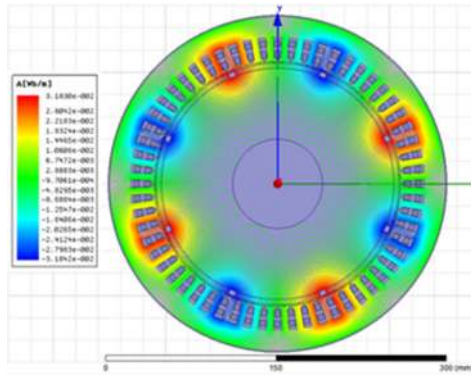


FIGURE 16. Flux line plot of the SSSRFP-PMSG.

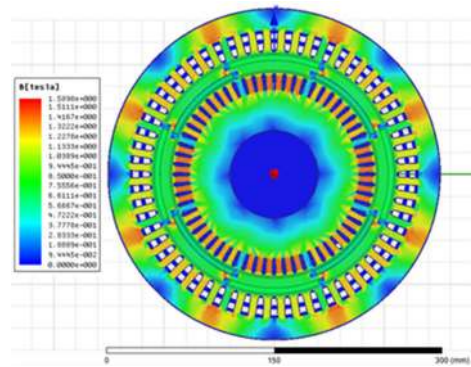


FIGURE 17. Flux density plot of NDSPPFP-PMSG.

density in the stator tooth portion is maximum. This portion of the machine is most sensitive to saturation. But, the value of flux density in this portion is below the 1.58 T, which ensures the optimal designing of the generator.

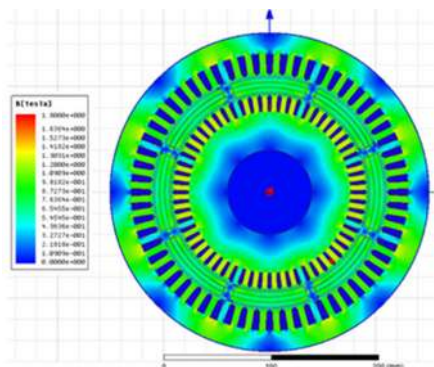


FIGURE 18. Flux density plot of DSEFPFP-PMSG.

Fig. 18 shows the flux density distribution in the DSEFPFP generator. It is clear from the plot that the flux density at different portions namely, outer stator yoke, outer stator tooth, rotor yoke, inner stator tooth, and inner stator yoke are 0.981T, 1.090 T, 0.872T, 1.309 T and 0.872 T respectively. From the above values of flux density, it is observed that the flux density in the stator tooth portion is maximum. This portion of the machine is most sensitive to saturation.

But, the value of flux density in this portion is below the 1.8 T, which ensures the optimal designing of the generator.

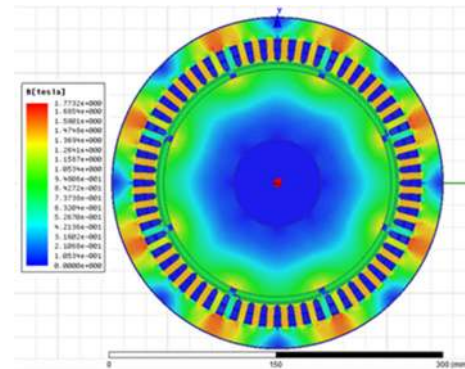


FIGURE 19. Flux density plot of SSSRFP-PMSG.

Fig. 19 shows the flux density distribution in the SSSRFP-PMSG generator. From the plot it clear that the flux density at different portions namely, outer stator yoke, outer stator tooth, rotor yoke is 0.948T, 1.474 T, 0.948 T respectively. It is observed from the above values of flux density that the flux density in the stator tooth portion is maximum. This portion of machine is most sensitive to saturation. But, the value of flux density in this portion is below 1.77T, which ensures the optimal designing of the generator.

V. RESULTS AND VALIDATION

The Dynamic Magnetic Circuit Model (DMCM) has been proposed to get the optimal performance of the proposed NDSPPFP-PMSG. To validate the predicted results, FEM analysis is done using Ansoft Maxwell software. In addition, to prove the performance superiority of the proposed NDSPPFP-PMSG, it is compared with two conventional generators namely, DSEFPFP-PMSG and SSSRFP-PMSG. For the performance analysis of the above-mentioned generators, FEM analysis are carried out owing to its high accuracy. The electromagnetic performance namely, airgap flux density, generated EMF, %THD of generated EMF, generated EMF vs speed, terminal voltage vs load current, electromagnetic torque developed on rotor vs time, %ripple content in the torque, and %efficiency vs load current are investigated below.

A. AIRGAP FLUX DENSITY

The proposed NDSPPFP-PMSG has two kind of magnetic poles namely, actual or real and pseudo-pole. The predicted inner airgap flux density obtained from DMCM for the actual pole and pseudo pole is found to be 563.5 milli-Tesla (mT) and 485.2 mT respectively, whereas that obtained from FEM is 569.8 mT for actual pole and 490.2 mT for pseudo-pole as shown in Fig. 20. It is found that the predicted results obtained is 1.105% and 1.0199% lesser than that obtained from FEM results for the actual and pseudo-pole respectively as shown in Table 3. The magnitude of inner airgap flux density for the DSEFPFP-PMSG is found to be 563 mT as

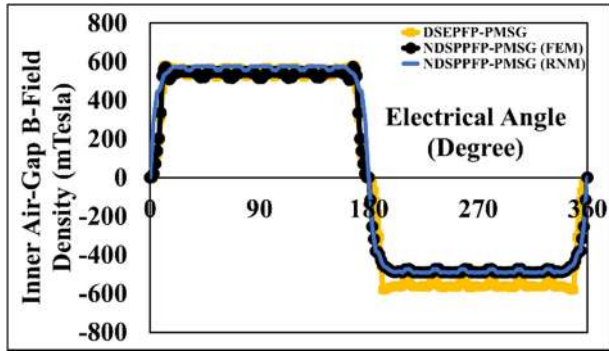


FIGURE 20. Inner air-gap flux density.

TABLE 3. Comparison Between Analytical and FEM Results obtained for NDSPPFP-PMSG.

	FEM Analysis	Analytical Method (DMCM)	% Difference
Inner Airgap Flux Density	569.8mT (real) 490.2mT (pseudo)	563.5mT (real) 485.2mT (pseudo)	1.105% (real) 1.0199% (pseudo)
Outer Airgap Flux Density	519.72mT (real) 474.05mT (pseudo)	512.3mT (real) 470.02mT(pseudo)	1.427% (real) 0.8501% (pseudo)
Inner Stator Generated EMF	140 volts	138.45 volts	1.107%
Outer Stator Generated EMF	305 volts	300.65 volts	1.426%
Inner Stator Terminal Voltage	128.232 volts	126.696 volts	1.197%
Outer Stator Terminal Voltage	290.993 volts	286.644 volts	1.494%
Torque developed	-212.5 Nm	-209.271 Nm	1.519%
%Efficiency	94.42%	94.351%	0.073%

shown in Fig. 20. It is found that the inner airgap flux density of DSEPFP-PMSG is lesser than the proposed NDSPPFP-PMSG. The values of inner airgap flux density are enlisted in Table 4.

Similarly, the predicted outer airgap flux density obtained from DMCM for the actual pole and pseudo pole is found to be 512.3 mT and 470.02 mT respectively, whereas that obtained from FEM is 519.72 mT for actual pole and 474.05mT for pseudo-pole as shown in Fig. 21. It is found that the predicted results obtained is 1.427% and 0.8501% lesser than that obtained from FEM results for the actual and pseudo-pole respectively as shown in Table 3. The magnitude of average outer airgap flux density for the DSEPFP-PMSG and SSSRFP-PMSG is found to be 514 mT and 711 mT respectively as shown in Fig. 21. It is found that the outer airgap flux density of DSEPFP-PMSG is lesser than the proposed NDSPPFP-PMSG, whereas that of SSSRFP -PMSG

TABLE 4. Comparative Performance Parameter for NDSPPFP-PMSG, DSEPFP-PMSG and SSSRFP-PMSG.

Parameter	NDSPPFP-PMSG	DSEPFP-PMSG	SSSRFP-PMSG	Unit
Power	12.576	10.394	10.593	kW
Inner Airgap flux density	0.5698 (real)	0.563	-	Tesla
Outer Airgap flux density	0.5197 (real)	0.514	0.711	Tesla
Inner Stator Voltage	140	130	-	Volts
%THD in inner stator EMF	40.4	34.82	-	-
%Voltage regulation for inner stator terminal	9.17	11.03	-	-
Outer stator voltage	305	260	370	Volts.
%THD in outer stator EMF	41.11	35.79	37.46	-
%Voltage Regulation for outer stator terminal	4.813	13.34	4.786	-
Stator Phase Current	6	6	6	Amps.
Cogging Torque	1.3	0.6	2.25	Nm
Torque developed on the rotor	-212.5	-177.5	-177	Nm
%ripple factor in the rotor torque	5.39	4.89	7.825	-
%Efficiency	94.42	93.42	95.35	-
Power-weight ratio	357.895	297.264	269.11	Watts/kg

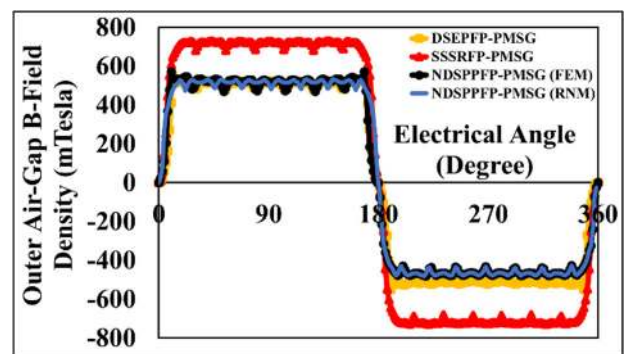


FIGURE 21. Outer air-gap flux density.

is greater than the proposed generator. The values of outer airgap flux density are enlisted in Table 4.

B. GENERATED EMF AND %THD

The inner stator generated EMF for the proposed NDSPPFP-PMSG obtained from DMCM is found to be 138.45 volts at 40 Hz whereas that obtained from FEM is 140 Volts at 40 Hz

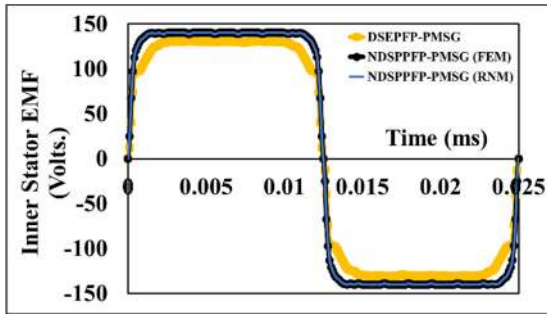


FIGURE 22. Inner stator generated EMF of NDSPPFP-PMSG and DSEFPFP-PMSG.

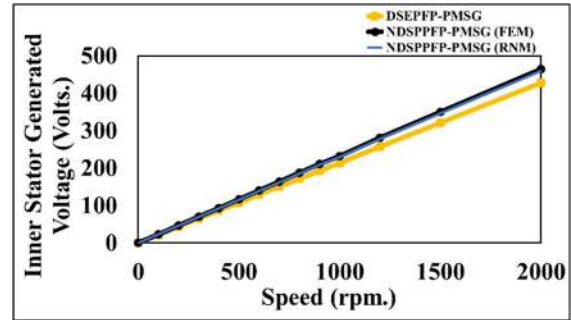


FIGURE 25. Inner stator generated EMF vs speed of NDSPPFP-PMSG and DSEFPFP-PMSG.

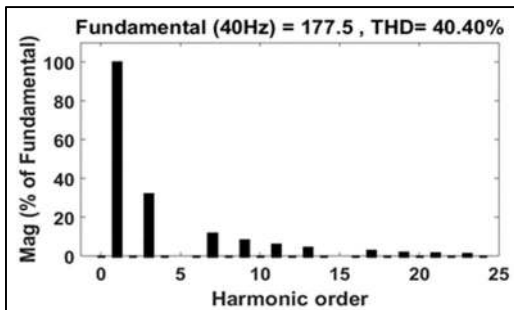


FIGURE 23. FFT analysis of Inner stator generated EMF of NDSPPFP-PMSG.

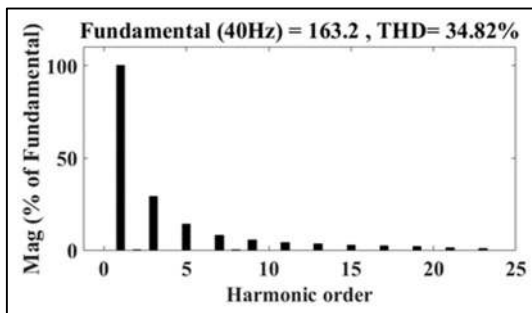


FIGURE 24. FFT analysis of the Inner stator generated EMF of DSEFPFP-PMSG.

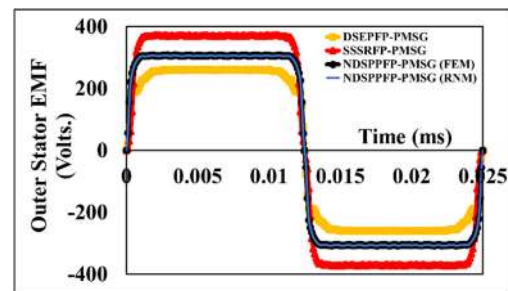


FIGURE 26. Outer stator generated EMF.

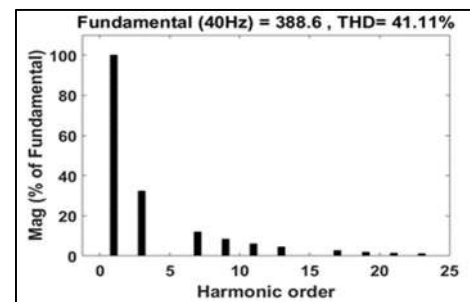


FIGURE 27. FFT analysis of the outer stator generated EMF of NDSPPFP-PMSG.

as shown in Fig. 22. The EMF obtained from DMCM is found to be 1.107 % lesser that FEM results as shown in Table 3. The inner stator generated EMF of DSEFPFP-PMSG is found to be 130 volts at 40 Hz as shown in Fig. 22. The %THD in the inner stator generated EMF is found to be 40.40% for NDSPPFP-PMSG and 34.82% for DSEFPFP-PMSG as shown in Fig. 23 and Fig. 24 respectively. From the %THD plot, it is clear that the harmonic content in the inner stator generated EMF of NDSPPFP-PMSG is higher because of the unequal magnitude of the airgap flux density in both the half cycles. It is also found that in the generated EMF, all the odd harmonics are present except the multiple of 5th harmonics. The values of inner stator generated EMF and their %THD are enlisted in Table 4.

The outer stator generated EMF for the proposed NDSPPFP-PMSG obtained from DMCM is found to be 300.65 volts at 40 Hz whereas that obtained from FEM is 305 Volts at 40 Hz as shown in Fig. 26. The EMF obtained from DMCM is found to be 1.426% lesser that FEM results as shown in Table 3. The outer stator generated EMF of DSEFPFP-PMSG and SSSRFP-PMSG is found to be 260 volts and 370 volts at 40 Hz respectively as shown in Fig. 26. The %THD in the outer stator generated EMF is found to be 41.11% for NDSPPFP-PMSG and 35.79% for DSEFPFP-PMSG as shown in Fig. 27 and Fig. 28 respectively.

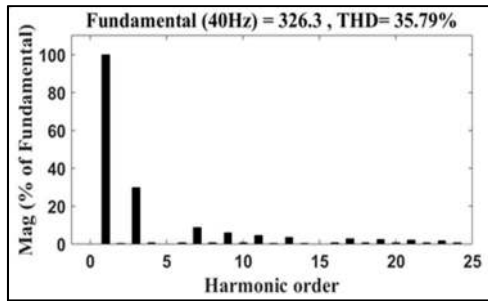


FIGURE 28. FFT analysis of the outer stator generated EMF of DSEPFP-PMSG.

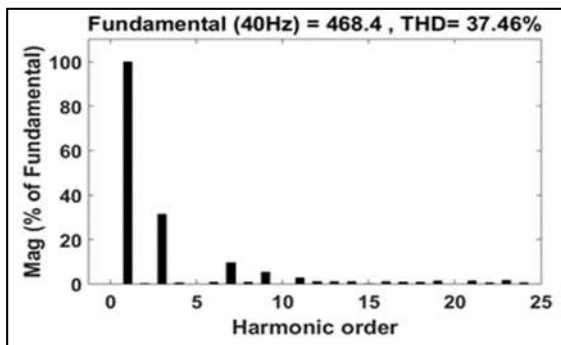


FIGURE 29. FFT analysis of the outer stator generated EMF of SSSRFP-PMSG.

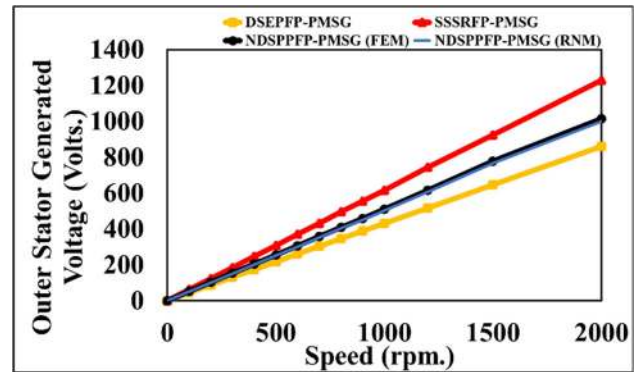


FIGURE 30. Outer stator generated EMF vs speed.

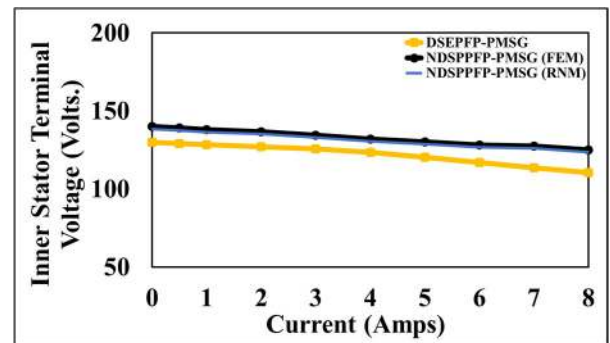


FIGURE 31. Inner stator terminal voltage vs current.

Similarly, the %THD in the generated EMF is found to be 37.46 % for the SSSRFP-PMSG as shown in Fig. 29. From the %THD plot it is clear that the harmonic content in the outer stator generated EMF of NDSPPFP-PMSG is highest because of unequal magnitude of the airgap flux density in both the half cycles. It is also found that in the generated EMF only the odd harmonics are present except the multiple of 5th harmonic. The values of inner and outer stator generated EMF and its %THD both are enlisted in Table 4. As shown in Fig. 20 and Fig. 21, the variation of the inner and outer airgap magnetic field densities in the proposed generator in both the half cycles are not equal due to which a high % THD is present in the generated EMFs. It can be reduced by sinusoidal shaping of the magnetic poles of the generator.

Fig. 30 shows the outer stator generated EMF vs speed plot of NDSPPFP, DSEPFP and SSSRFP-PMSG. It is observed that predicted and FEM results of the NDSPPFP-PMSG are linear. Similarly, the curve for DSEPFP-PMSG and SSSRFP-PMSG are also linear. SSSRFP-PMSG has the highest slope whereas the DSEPFP-PMSG has the lowest slope.

C. TERMINAL VOLTAGE AND %VOLTAGE REGULATION

The inner stator terminal voltage of NDSPPFP-PMSG obtained from DMCM and FEM is 126.696 volts and 128.232 volts respectively at rated current of 6 Amps. The predicted inner terminal voltage is found to be 1.197% less than that obtained from FEM as shown in Table 3.

Fig. 31 shows the variation of the inner stator terminal voltage with load current of NDSPPFP-PMSG and DSEPFP-PMSG. The terminal voltage for both the generators are found to droop during loading conditions. These drooping characteristics of terminal voltage is due to the armature reaction and winding parameters. It is found that the % voltage regulation for the inner stator of NDSPPFP-PMSG and DSEPFP-PMSG is 9.17 and 11.03 respectively. It can be concluded that the proposed generator has a better loading capability than DSEPFP-PMSG.

Similarly, the outer stator terminal voltage of NDSPPFP-PMSG obtained from DMCM and FEM is 286.644 volts and 290.993 volts respectively. The predicted outer terminal voltage is found to be 1.494% less than that obtained from FEM as shown in Table 3.

Fig. 32 shows the variation of the outer stator terminal voltage with load current of NDSPPFP, DSEPFP and SSSRFP-PMSG. The %voltage regulation for the outer stator of NDSPPFP-PMSG, DSEPFP-PMSG and SSSRFP-PMSG is 4.813, 13.34 and 4.786 respectively. The terminal voltage for all the generators is found to droop during loading conditions. These drooping characteristics of outer stator terminal voltage is due to the armature reaction and passive parameters of the windings. It can be concluded that the DSEPFP-PMSG has a poor loading capability whereas the NDSPPFP-PMSG and SSSRFP-PMSG have an almost similar loading capability. The values of %voltage regulation of outer stator terminal voltage is enlisted in Table 4.

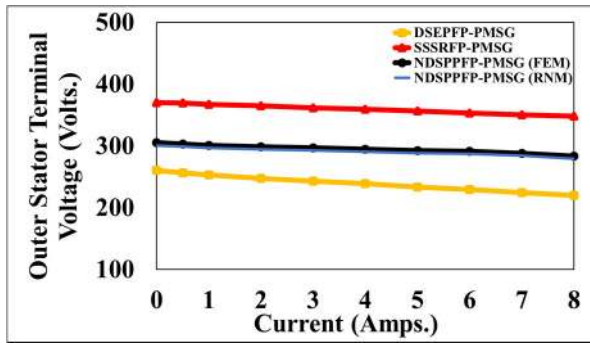


FIGURE 32. Outer stator terminal voltage vs current.

D. ELECTROMAGNETIC TORQUE AND %RIPPLE CONTENT

The NDSPPFP-PMSG has torque of magnitude 209.271 Nm and 212.5 Nm obtained from analytical and FEM analysis respectively as shown in Table 3. It is observed that the predicted magnitude of torque is 1.519% less than that of FEM magnitude.

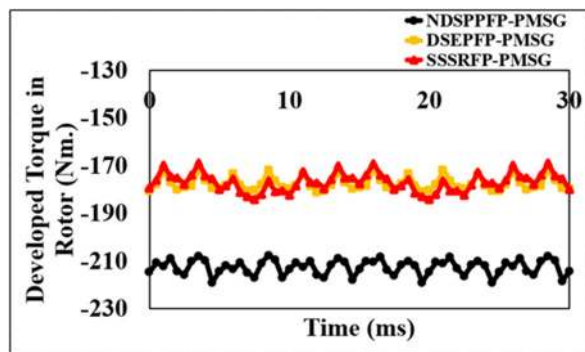


FIGURE 33. Developed torque in the rotor.

Fig. 33 shows the electromagnetic torque developed in the rotors of all the three generators. The magnitude of torque developed for DSEFPF and SSSRFP-PMSG are 177.5 Nm and 177 Nm respectively. Also, the %ripple content of NDSPPFP, DSEFPF and SSSRFP-PMSG are 5.39, 4.89 and 7.825 respectively. From the %ripple factor of torque it is clear that the DSEFPF-PMSG has less ripple factor compared to the proposed generator. It is because, the magnets are embedded inside the rotor and thus no PM-PM slotting effect appeared in this model. In order to reduce the %ripple factor of torque in the proposed generator, the gap between adjacent actual and pseudo-pole should be minimum.

The torque developed in all three generators and their %ripple factors are enlisted in Table 4.

E. EFFICIENCY

The efficiency of NDSPPFP-PMSG obtained from DMCM is 94.351% and from FEM analysis is 94.42% as shown in Fig. 34. The predicted efficiency is 0.073% less than the FEM analysis as enlisted in Table 3.

The efficiency of SSSRFP-PMSG is found to be the highest i.e. 95.35 % and that of DSEFPF-PMSG is found to be

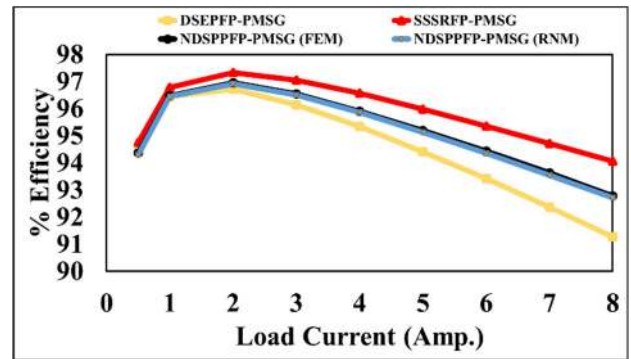


FIGURE 34. Efficiency vs load current.

93.42% which is the lowest amongst all as shown in Fig. 34. The efficiency is calculated at the rated current of 6 Amps., neglecting the friction and windage loss of the machine. Furthermore, as the power density increases, the dominance of lower order harmonics in the load current increases due to which the eddy current in PMs also increases. But the contribution of losses compared to the copper and core losses is very less so it can also be neglected while calculating the efficiency. The efficiency of all three generators are enlisted in Table 4.

For design and analysis of machines, the analytical method is more popular as it gives fast results and to validate the analytical results the FEM analysis is considered. Though FEM analysis is slow, but it gives accurate results. In [52], it has been investigated that the difference between results of FEM and analytical analysis is within 3% where they have considered parameters such as, leakage flux, saturation effect and core material. Similarly, in [53] the difference obtained is about 2%. Here, only leakage flux parameter is considered. While, in the proposed model, the difference between FEM and analytical method (DMCM) results is less than 1.5% where saturation effect, core material, leakage flux and MMF sources parameters are used. Thus, it is figured out that the dynamic magnetic circuit model opted in this paper is better compared to the other magnetic circuit model investigated.

VI. CONCLUSION

In this paper, the Novel Dual Stator Pseudo-Pole Five Phase Permanent Magnet Synchronous Generator (NDSPPFP-PMSG) has been proposed for wind power application. The novelty of the generator is due to the special arrangement of the magnet. Here, eight poles of magnets are formed by using only four poles of actual magnets on both the surfaces of the rotor. This helps in saving the PM material and thus reduces the overall cost of the generator. For designing and performance optimization, Dynamic Magnetic Circuit Model (DMCM) has been proposed for the NDSPPFP-PMSG. The predicted results are then validated with the results obtained from FEM. The results such as airgap flux density, generated EMF, generated voltage vs speed, terminal voltage vs load current and %efficiency vs load current are compared and the error difference found is within 1.5%.

To prove the superiority of the proposed generator, it is compared with two conventional generators namely, Dual Stator Embedded-Pole Five Phase (DSEFP-PMSG) and Single Stator Single Rotor Five Phase (SSSRFP-PMSG). The FEM results of these three generators are compared and it is found that the flux density in the inner airgap of the proposed NDSPPFP-PMSG is found higher than the DSEFP-PMSG. It is also found that the outer airgap density of the SSSRFP-PMSG is highest (0.711 T). The inner stator generated EMF for the proposed generator is found to be the highest. Similarly, for the outer stator, the generated EMF of the SSSRFP-PMSG is found to be the highest. The generated voltage vs speed plots of all the three generators increase linearly. The terminal voltage vs load current plot shows drooping characteristics for all the generators. From the %voltage regulation, it can be concluded that the proposed generator has better loading capability for the inner stator-rotor system whereas, the loading capability of the outer stator-rotor system for the proposed generator and SSSRFP-PMSG are nearly same. The developed torque is highest for the proposed generator (212.5 Nm). From %ripple content of the torque, it is clear that the DSEFP generator has the lowest ripple factor because the magnets are embedded inside the rotor. From the efficiency vs load current plot, it can be concluded that the SSSRFP-PMSG has the highest efficiency of 95.35% and the efficiency of the proposed generator is 94.42%. The efficiency is calculated at the rated current of 6 amps with the assumption of neglecting the friction, windage and PM eddy current loss of the machine.

The power densities (power to weight ratio) for NDSPPFP, DSEFP and SSSRFP-PMSG are found to be 357.895 watt/kg, 297.264 watt/kg and 269.11 watts/kg respectively. It is concluded that, for the same volume of the generators, the power density for the proposed NDSPPFP-PMSG is found to be the highest. On the basis of the above performance and power density it is concluded that, our proposed NDSPPFP-PMSG is most suitable generator for the wind power application.

ACKNOWLEDGMENT

The authors are thankful to the Department of Electrical Engineering, Jorhat Engineering College, Assam and friends and faculties of the Department of Electrical Engineering, IIT (BHU) Varanasi.

REFERENCES

- [1] R. M. Elavarasan, G. M. Shafiqullah, S. Padmanaban, N. M. Kumar, A. Annam, A. M. Vetrivelvan, L. Mihet-Popa, and J. B. Holm-Nielsen, "A comprehensive review on renewable energy development, challenges, and policies of leading Indian States with an international perspective," *IEEE Access*, vol. 8, pp. 74432–74457, 2020.
- [2] E. Fouché and A. Brent, "Explore, design and act for sustainability: A participatory planning approach for local energy sustainability," *Sustainability*, vol. 12, no. 862, pp. 1–17, 2020.
- [3] F. Blaabjerg and K. Ma, "Wind energy systems," *Proc. IEEE*, vol. 105, no. 11, pp. 2116–2131, Nov. 2017.
- [4] B. K. Bose, "Power electronics, smart grid, and renewable energy systems," *Proc. IEEE*, vol. 105, no. 11, pp. 2011–2018, Nov. 2017.
- [5] V. Yaramasu, B. Wu, P. C. Sen, S. Kouro, and M. Narimani, "High-power wind energy conversion systems: State-of-the-art and emerging technologies," *Proc. IEEE*, vol. 103, no. 5, pp. 740–788, May 2015.
- [6] K. Deveci, B. Barutçu, E. Alpman, A. Ta cıkaraoğlu, and O. Erdiñç, "Electrical layout optimization of onshore wind farms based on a two-stage approach," *IEEE Trans. Sustain. Energy*, vol. 11, no. 4, pp. 2407–2416, Oct. 2020.
- [7] L. Ziegler, E. Gonzalez, T. Rubert, U. Smolka, and J. J. Meleró, "Lifetime extension of onshore wind turbines: A review covering Germany, Spain, Denmark, and the U.K.," *Renew. Sustain. Energy Rev.*, vol. 82, pp. 1261–1271, Feb. 2018.
- [8] S. Kumar, R. K. Saket, D. K. Dheer, J. Holm-Nielsen, and P. Sanjeevikumar, "Reliability enhancement of electrical power system including impacts of renewable energy sources: A comprehensive review," *IET Gener., Transmiss. Distrib.*, vol. 14, no. 10, pp. 1799–1815, May 2020.
- [9] S. Pfaffel, S. Faulstich, and K. Rohrig, "Performance and reliability of wind turbines: A review," *Energies*, vol. 10, no. 11, p. 1904, Nov. 2017.
- [10] J. H. Chow and J. J. Sanchez-Gasca, "Wind power generation and modeling," in *Power System Modeling, Computation, and Control*, 1st ed. Hoboken, NJ, USA: Wiley, 2020, pp. 487–530.
- [11] Y.-W. Lin, Y.-H. Wu, C.-C. Chen, and J.-L. Dong, "Wind energy in Taiwan and the standard of communication for wind turbines," *Int. J. Smart Grid Clean Energy*, vol. 4, no. 4, pp. 328–335, Oct. 2015.
- [12] J. E. Diffendorfer, L. A. Kramer, Z. H. Ancona, and C. P. Garrity, "Onshore industrial wind turbine locations for the United States up to March 2014," *Sci. Data*, vol. 2, no. 1, pp. 1–8, 2015.
- [13] R. A. Gupta, B. Singh, and B. Bhushan Jain, "Wind energy conversion system using PMSG," in *Proc. Int. Conf. Recent Develop. Control, Autom. Power Eng. (RDCAPE)*, Mar. 2015, pp. 199–203.
- [14] D. B. de Alencar, C. De M. Affonso, R. C. L. de Oliveira, J. L. M. Rodríguez, J. C. Leite, and J. C. R. Filho, "Different models for forecasting wind power generation: Case study," *Energies*, vol. 10, no. 12, pp. 1–27, 2017.
- [15] J. Tian, D. Zhou, C. Su, F. Blaabjerg, and Z. Chen, "Maximum energy yield oriented turbine control in PMSG-based wind farm," *J. Eng.*, vol. 2017, no. 13, pp. 2455–2460, Jan. 2017.
- [16] R. T. Sanchez and A. M. Rios, "Modeling and control of a wind turbine," in *Bond Graphs for Modelling, Control and Fault Diagnosis of Engineering Systems*. Cham, Switzerland: Springer, 2017, ch. 15, pp. 547–585.
- [17] D. K. V. Sagiraju, Y. P. Obulesu, and S. B. Choppavarapu, "Dynamic performance improvement of standalone battery integrated PMSG wind energy system using proportional resonant controller," *Eng. Sci. Technol., Int. J.*, vol. 20, no. 4, pp. 1353–1365, Aug. 2017.
- [18] P. Han, M. Cheng, Y. Jiang, and Z. Chen, "Torque/power density optimization of a dual-stator brushless doubly-fed induction generator for wind power application," *IEEE Trans. Ind. Electron.*, vol. 64, no. 12, pp. 9864–9875, Dec. 2017.
- [19] M. Rajvikram, P. Renuga, G. A. Kumar, and K. Bavithra, "Fault ride-through capability of permanent magnet synchronous generator based wind energy conversion system," *Power Res.*, vol. 12, pp. 531–538, Jul. 2016.
- [20] A. B. Kjaer, S. Korsgaard, S. S. Nielsen, L. Demsa, and P. O. Rasmussen, "Design, fabrication, test, and benchmark of a magnetically geared permanent magnet generator for wind power generation," *IEEE Trans. Energy Convers.*, vol. 35, no. 1, pp. 24–32, Mar. 2020.
- [21] G. van de Kaa, M. van Ek, L. M. Kamp, and J. Rezaei, "Wind turbine technology battles: Gearbox versus direct drive—opening up the black box of technology characteristics," *Technol. Forecasting Social Change*, vol. 153, Apr. 2020, Art. no. 119933.
- [22] M. Rajvikram, P. Renuga, and M. Swathisriranjani, "Fuzzy based MPPT controller's role in extraction of maximum power in wind energy conversion system," in *Proc. Int. Conf. Control, Instrum., Commun. Comput. Technol. (ICCICCT)*, Dec. 2016, pp. 713–719.
- [23] R. M. Pindoriya, A. Usman, B. S. Rajpurohit, and K. N. Srivastava, "PMSG based wind energy generation system: Energy maximization and its control," in *Proc. 7th Int. Conf. Power Syst. (ICPS)*, Dec. 2017, pp. 376–381.
- [24] Y. Zou and J. He, "Maximum power point tracking (MPPT) of sensorless PMSG wind power system," in *Proc. IEEE Energy Convers. Congr. Expo. (ECCE)*, Sep. 2016, pp. 1–6.
- [25] P. T. Huynh, P. J. Wang, and A. Banerjee, "An integrated permanent-magnet-synchronous generator-rectifier architecture for limited-speed-range applications," *IEEE Trans. Power Electron.*, vol. 35, no. 5, pp. 4767–4779, May 2020.

- [26] Y.-C. Chang, H.-C. Chang, and C.-Y. Huang, "Design and implementation of the Permanent-magnet synchronous generator drive in wind generation systems," *Energies*, vol. 11, no. 7, p. 1634, Jun. 2018.
- [27] S. Nanda and M. Sengupta, "Design, fabrication and analytical investigations on a permanent magnet synchronous generator," in *Proc. IEEE Int. Conf. Power Electron., Drives Energy Syst. (PEDES)*, Dec. 2014, pp. 1–4.
- [28] V. B. Petkar, "Design of electrical PM generator with doublesided stator and single rotor (DSSR) technology—Part I," *Int. J. Adv. Res. Electr., Electron. Instrum. Eng.*, vol. 4, no. 10, pp. 8130–8134, Oct. 2015.
- [29] S. M. Salihu, N. Mison, L. Md Othman, and T. Hanamoto, "Power density evaluation of a novel double-stator magnetic geared permanent magnet generator," *Prog. Electromagn. Res. B*, vol. 80, pp. 19–35, 2018.
- [30] A. R. Dehghanzadeh and V. Behjat, "Dynamic modeling and experimental validation of a dual-stator PMSG for low speed applications," *Gazi Univ. J. Sci.*, vol. 28, no. 2, pp. 275–283, 2015.
- [31] Y. Chen and B. Liu, "Design and analysis of a five-phase fault-tolerant permanent magnet synchronous motor for aerospace starter-generator system," *IEEE Access*, vol. 7, pp. 135040–135049, 2019.
- [32] A. Monni, I. Marongiu, A. Serpi, and A. Damiano, "Design of a fractional slot multi-phase PMSG for a direct-drive wind turbine," in *Proc. Int. Conf. Electr. Mach. (ICEM)*, Sep. 2014, pp. 2087–2093.
- [33] D. Yu, X. Y. Huang, Y. T. Fang, and J. Zhang, "Design and comparison of interior permanent magnet synchronous traction motors for high speed railway applications," in *Proc. IEEE Workshop Electr. Mach. Design, Control Diagnosis (WEMDCD)*, Apr. 2017, pp. 58–62.
- [34] K.-H. Shin, H.-I. Park, K.-H. Kim, S.-M. Jang, and J.-Y. Choi, "Magnet pole shape design for reduction of thrust ripple of slotless permanent magnet linear synchronous motor with arc-shaped magnets considering end-effect based on analytical method," *AIP Adv.*, vol. 7, no. 5, May 2017, Art. no. 056656.
- [35] H. Fang and D. Wang, "Design of permanent magnet synchronous generators for wave power generation," *Trans. Tianjin Univ.*, vol. 22, no. 5, pp. 396–402, Oct. 2016.
- [36] A. Damiano, A. Floris, G. Fois, M. Porru, and A. Serpi, "Modelling and design of PM retention sleeves for high-speed PM synchronous machines," in *Proc. 6th Int. Electr. Drives Prod. Conf. (EDPC)*, Nov. 2016, pp. 118–125.
- [37] D. Xu, X. Wang, and G. Li, "Optimization design of the sleeve for high speed permanent magnet machine," in *Proc. IEEE 11th Conf. Ind. Electron. Appl. (ICIEA)*, Jun. 2016, pp. 2531–2535.
- [38] W. Li, H. Qiu, X. Zhang, J. Cao, S. Zhang, and R. Yi, "Influence of rotor-sleeve electromagnetic characteristics on high-speed permanent-magnet generator," *IEEE Trans. Ind. Electron.*, vol. 61, no. 6, pp. 3030–3037, Jun. 2014.
- [39] X. Hu, Y. Lia, and L. Luo, "The influence of air gap thickness between the stator and rotor on nuclear main pump," in *Proc. 9th ICAE Energy Procedia*, vol. 142, 2017, pp. 259–264.
- [40] P. Arumugam and C. Gerada, "Short term duty electrical machines," in *Proc. 12th Int. Conf. Electr. Mach. (ICEM)*, Sep. 2016, pp. 2676–2681.
- [41] V. Bilyi and D. Gerling, "Design of high-efficiency interior permanent magnet synchronous machine with stator flux barriers and single-layer concentrated windings," in *Proc. IEEE Int. Electr. Mach. Drives Conf. (IEMDC)*, May 2015, pp. 1177–1183.
- [42] S. Ma, X. Zhang, Q. Du, L. Shi, and X. Meng, "Optimization design of a new type of interior permanent magnet generator for electric vehicle range extender," *J. Electr. Comput. Eng.*, vol. 2019, pp. 1–10, May 2019.
- [43] Y. Yang, S. M. Castano, R. Yang, M. Kasprzak, B. Bilgin, A. Sathyan, H. Dadkhah, and A. Emadi, "Design and comparison of interior permanent magnet motor topologies for traction applications," *IEEE Trans. Transport. Electrific.*, vol. 3, no. 1, pp. 86–97, Mar. 2017.
- [44] V. Bilyi and D. Gerling, "Design of high-efficiency interior permanent magnet synchronous machine with stator flux barriers and single-layer concentrated windings," in *Proc. IEEE Int. Electr. Mach. Drives Conf. (IEMDC)*, May 2015, pp. 1177–1183.
- [45] G. Choi and T. M. Jahns, "Interior permanent magnet synchronous machine rotor demagnetization characteristics under fault conditions," in *Proc. IEEE Energy Convers. Congr. Expo.*, Sep. 2013, pp. 2500–2507.
- [46] S. M. Barrans, M. M. J. Al-Ani, and J. Carter, "Mechanical design of rotors for permanent magnet high-speed electric motors for turbocharger applications," *IET Electr. Syst. Transp.*, vol. 7, no. 4, pp. 278–286, Dec. 2017.
- [47] G. Cooke and K. Atallah, "'Pseudo' direct drive electrical machines with alternative winding configurations," *IEEE Trans. Magn.*, vol. 53, no. 11, Nov. 2017, Art. no. 8111608.
- [48] R. R. Kumar, R. K. Srivastava, S. K. Singh, and R. K. Saket, "Design, control and experimental investigation of fault-tolerant five phase PMSG for wind power application," *Int. J. Mech. Prod. Eng. Res. Develop.*, vol. 8, no. 4, pp. 1107–1122, 2018.
- [49] R. R. Kumar, S. K. Singh, and R. K. Srivastava, "Design analysis of radial flux dual stator five phase permanent magnet synchronous generator," in *Proc. IEEE Int. Conf. Power Electron., Drives Energy Syst. (PEDES)*, Dec. 2014, pp. 1–6.
- [50] H. Tiegna, Y. Amara, and G. Barakat, "Overview of analytical models of permanent magnet electrical machines for analysis and design purposes," *Math. Comput. Simul.*, vol. 90, pp. 162–177, Apr. 2013.
- [51] E. ManaaBarhoumi, F. Wurtz, C. Chillet, and B. Ben Salah, "Reluctance network model for linear switched reluctance motor," in *Proc. IEEE 12th Int. Multi-Conf. Syst., Signals Devices (SSD)*, Mar. 2015, pp. 1–4.
- [52] M. L. Guyadec, L. Gerbaud, E. Vinot, V. Reinbold, and C. Dumont, "Use of reluctance network modelling and software component to study the influence of electrical machine pole number on hybrid electric vehicle global optimization," *Math. Comput. Simul.*, vol. 158, pp. 79–90, Apr. 2019.
- [53] D.-K. Lim and J.-S. Ro, "Analysis and design of a delta-type interior permanent magnet synchronous generator by using an analytic method," *IEEE Access*, vol. 7, pp. 85139–85145, 2019.
- [54] M. A. Hernandez-Rodriguez, R. Iracheta-Cortez, N. Flores-Guzman, E. Hernandez-Mayoral, R. Gomez-Torres, and W. Durante-Gomez, "Designing a transverse flux PMSG with analytical methods for applications in wind turbines," in *Proc. IEEE 38th Central Amer. Panama Conv.*, Nov. 2018, pp. 1–9.
- [55] A. C. Barmpatza and J. C. Kappatou, "Finite element method investigation and loss estimation of a permanent magnet synchronous generator feeding a non-linear load," *Energies*, vol. 11, no. 12, p. 3404, Dec. 2018.
- [56] R. R. Kumar, S. K. Singh, and R. K. Srivastava, "Effect of magnetic trajectories in a magnetically coupled dual stator five phase PMSG," in *Proc. IEEE Int. Conf. Ind. Technol. (ICIT)*, Mar. 2015, pp. 720–725.



RAJA RAM KUMAR received the B.Tech. degree in electrical engineering from the West Bengal University of Technology, Kolkata, India, in 2010, and the M.Tech. and Ph.D. degrees in electrical machines and drives from the Indian Institute of Technology (BHU) Varanasi, India, in 2012 and 2018, respectively. He is currently working as an Assistant Professor with the Department of Electrical Engineering, Jorhat Engineering College, Assam. He is the author of several research papers which are published in international/national journals and conference proceedings. His current research interests include renewable energy, electrical machines, electric drives, as well as power electronic converter design and control. He was the Chair-Person of the Student Branch of the IEEE-IAS at IIT (BHU) Varanasi from 2016 to 2018. He received the Institute Research Award from IIT (BHU) Varanasi in 2016 and the Second Prize Paper Award in the IACC Annual Meeting 2018 at Portland during IAS Annual Meeting.



PRIYANKA DEVI was born in Sibsagar, Assam, India, in 1997. She received the B.E. degree in electrical engineering from the Jorhat Engineering College, Jorhat, Assam, India, in 2020. Her research interests include renewable energy, electrical machines, electric drives, and permanent magnet generators. She has published several book chapters and research papers in international/national journals and conference proceedings.



CHANDAN CHETRI was born in Guwahati, Assam, India, in 1997. He received the B.E. degree in electrical engineering from the Jorhat Engineering College, Jorhat, Assam, India, in 2020. His research interests include renewable energy, electrical machines, electric drives, and permanent magnet generators. He has published several book chapters and research papers in international/national journals and conference proceedings.



AANCHAL SINGH S. VARDHAN received the B.Tech. degree in electrical engineering from Sam Higginbottom University of Agriculture, Technology and Sciences, Allahabad, India, in 2019. She is currently pursuing the M.E. degree in electrical engineering with the specialization in power electronics with Shri G.S. Institute of Technology and Science, Indore, India, affiliated to Rajiv Gandhi University of Technology, Bhopal, India. Her innovative research work entitled “Movable Solar Power Generator” has been nominated for prestigious GYTI Award - 2020 at Rashtrapati Bhavan, New Delhi, India. She has published many research papers in reputed international journals and conference proceedings. Her research interests include renewable energy, wind energy conversion systems, DFIG controller design, design of synchronous generator, and modern aspects of power electronics.



RAJVIKRAM MADURAI ELAVARASAN received the B.E. degree in electrical and electronics engineering from Anna University, Chennai, India, and the M.E. degree in power system engineering from the Thiagarajar College of Engineering, Madurai. He worked as an Associate Technical Operations at the IBM Global Technology Services Division. He was a gold medalist of the master's degree. He worked as an Assistant Professor with the Department of Electrical and Electronics Engineering, Sri Venkateswara College of Engineering, Chennai. He is currently working as a Design Engineer with the Electrical and Automotive Parts Manufacturing Unit, AA Industries, Chennai. He has published papers in international journals, and international and national conferences. His areas of interest include solar PV cooling techniques, renewable energy and smart grids, wind energy research, power system operation and control, artificial intelligence, control techniques, and demand-side management. He is a recognized reviewer in reputed journals namely the IEEE SYSTEMS, IEEE ACCESS, IEEE Communications Magazine, International Transactions on Electrical Energy Systems (Wiley), Energy Sources, Part A: Recovery, Utilization and Environmental Effects (Taylor and Francis), Scientific Reports (Springer Nature), Chemical Engineering Journal (Elsevier), and CFD Letters and 3 Biotech (Springer).



LUCIAN MIHET-POPA (Senior Member, IEEE) was born in 1969. He received the bachelor's degree in electrical engineering, the master's degree in electric drives and power electronics, and the Ph.D. and Habilitation degrees in electrical engineering from the Politehnica University of Timisoara, Romania, in 1999, 2000, 2002, and 2015, respectively. Since 2016, he has been working as a Full Professor in energy technology with the Østfold University College, Norway. From 1999 to 2016, he was with the Politehnica University of Timisoara. He has also worked as a Research Scientist with Danish Technical University from 2011 to 2014, and also with Aalborg University, Denmark, from 2000 to 2002. He held a postdoctoral position with Siegen University, Germany, in 2004. He is also the Head of the Research Lab “Intelligent Control of Energy Conversion and Storage Systems” and is one of the Coordinators of the Master's degree Program in “Green Energy Technology” with the Faculty of Engineering, Østfold University College. He has published more than 130 papers in national and international journals and conference proceedings, and ten books. He has served as a scientific and technical program committee member for many IEEE conferences. He has participated in more than 15 international grants/projects, such as FP7, EEA, and Horizon 2020. He has been awarded more than ten national research grants. His research interests include modeling, simulation, control, and testing of energy conversion systems, and distributed energy resources (DER) components and systems, including battery storage systems (BSS) [for electric vehicles and hybrid cars and vanadium redox batteries (VRB)] and energy efficiency in smart buildings and smart grids. He was invited to join the Energy and Automotive Committees by the President and the Honorary President of the Atomium European Institute, working in close cooperation with—under the umbrella—the EC and EU Parliament, and was also appointed as the Chairman of AI4People, Energy Section. Since 2017, he has been a Guest Editor of five special issues of *Energies* (MDPI), *Applied Sciences*, *Majlesi Journal of Electrical Engineering*, and *Advances in Meteorology journals*.



R. K. SAKET (Senior Member, IEEE) is currently with the Department of Electrical Engineering, Indian Institute of Technology (BHU) Varanasi, India. He has more than 20 years of academic and research experience. He is the author/coauthor of approximately 110 scientific articles, book chapters, and research papers in the prestigious international journals and conference proceedings. His research interests include power system reliability, electrical machines and drives, reliability engineering, induction generators, DFIG controller design, and renewable energy systems. He is a Fellow of the Institution of Engineers (India) and a member of the IET (U.K.). He has received many awards, honors, and recognition for his academic and research contributions, including the prestigious GYTI Award-2018 by the Hon'ble President of India at New Delhi, India; Design Impact Award-2018 by Padma Vibhushan Ratan Tata at Mumbai, India; and Nehru Encouragement Award by M.P. State Government, Bhopal, India. He is an Associate Editor of the *IET – Renewable Power Generation* (UK), and an Editorial Board Member of the *Engineering, Technology & Applied Science Research* (Greece), and *Journal of Electrical Systems* (France).

...